mountain range, NW India, and its hinterland: the U–Pb and Hf isotope record of detrital zircon. *Precambrian Res.*, 2011, **187**, 155–164.

27. Dwivedi, A. K., Pandey, U. K., Murugan, C., Bhatt, A. K., Ramesh Babu, P. V. and Joshi, M., Geochemistry and geochronology of A-type Barabazar granite – implications on the geodynamics of the South Purulia Shear Zone, *Singhbhum craton*, Eastern India. *J. Geol. Soc. India*, 2011, **77**, 527–838.

28. Pandey, B. K., Krishna, V., Pandey, U. K. and Sastry, D. V. L. N., Radiometric dating of uranium mineralisation in the Proterozoic basins of eastern Dharwar craton, South India. In Proceedings of the International Conference on Peaceful Uses of Atomic Energy, New Delhi, 2009, vol. 1, pp. 116–117.

29. Rai, A. K., Pandey, U. K., Zakaulla, S. and Parihar, P. S., New Pb–Pb (PbSL) age of dolomites from Vempalle Formation, Lower Cuddapah Supergroup, Kadapa, India: implication on age of uranium mineralization. *J. Geol. Soc. India*, 2015, **86**, 131–136.

30. Bhowmik, S. K., Bernhardt, H.-J. and Dasgupta, S., Grenvillian age high-pressure upper amphibolite–granulite metamorphism in the Aravalli–Delhi Mobile Belt, northwestern India: new evidence from monazite chemical age and its implication. *Precambrian Res.*, 2010, **178**, 168–184.

31. Meert, J. G. *et al.*, Precambrian crustal evolution of Peninsular India: a 3.0 billion year odyssey. *J. Asian Earth Sci.*, 2010, **39**, 482–515.

Constraints on source parameters of the 25 April 2015, M_w = 7.8 Gorkha, Nepal earthquake from synthetic aperture radar interferometry

K. M. Sreejith[1,*], P. S. Sunil[2], Ritesh Agrawal[1], D. S. Ramesh[2] and A. S. Rajawat[1]

[1]Geosciences Division, Space Applications Centre (ISRO), Ahmedabad 380 015, India
[2]Indian Institute of Geomagnetism (DST), Navi Mumbai 410 218, India

We present InSAR observations of the co-seismic deformation caused by the M_w 7.8 Gorkha, Nepal earthquake. Analysis of Sentinel-1 data revealed about 100 × 100 sq. km surface deformation with ~1 m

*For correspondence. (e-mail: sreejith81@gmail.com)

upliftment near Kathmandu, and ~0.8 m subsidence towards north along the line of sight of the satellite. The maximum deformation is observed about 40 km east–southeast of the epicentre, suggesting eastward propagation of the rupture. Elastic dislocation modelling revealed that the overall rupture occurred on a 170 km long, 60 km wide fault along the strike (286°) and dipping north (dip = 15°) with large amount of slip (4.5 m) confined to the centre (95 × 22 sq. km) and less slip (0.25 m) on the surrounding part of the fault plane. The corresponding moment magnitude is M_w 7.75. The area, depth and dip of the modelled fault plane are fairly consistent and overlap with the location of mid-crustal ramp in the Main Himalayan Thrust. We infer that the earthquake was possibly caused by the release of inter-seismic strain energy accumulated in the environs of mid-crustal ramp due to plate boundary forces.

THE catastrophic 25 April 2015 Gorkha, Nepal earthquake of magnitude M_w 7.8 located between Pokhara and Kathmandu (28.147°N and 84.708°E)[1,2] is one of the largest earthquakes to have struck Nepal since the 1934 Nepal-Bihar earthquake of M_w 8.2 (ref. 3). The earthquake caused widespread destruction in Nepal and parts of India and China with the total death toll exceeding 9000 and also injuring 23,000 in an area inhabited by about 8 million people. Moment tensor solutions from telesiesmic data suggest that the Nepal earthquake occurred on a 10–20° dipping sub-horizontal blind thrust fault at about 15 km depth with a strike of 290° from the north[1]. The M_w 7.8 event was followed by 553 aftershocks with magnitude >4, including two events having magnitudes 6.1 and 6.6 on the same day[4,5]. The largest aftershock occurred on 12 May 2015, about 150 km east of the main shock (Figure 1).

Of the several large, devastating historical earthquakes that occurred in the Himalayan region, only four were instrumentally recorded: the 1897 Shillong Plateau, 1905 Kangra, 1934 Nepal–Bihar and the 1950 Assam earthquakes (Figure 1). These are the largest known earthquakes to have occurred at the intersection of basement and the décollement thrust faults that ruptured ~1400 km of the Himalayan detachment[6]. However, geodetic data of these earthquakes were either incomplete or not available[7], and hence the epicentral location and source parameters of these earthquakes remain elusive. Therefore, precise measurement of the surface deformation caused by the 2015 Nepal earthquake has special importance from the perspective of tectonics of large earthquakes in the Himalaya. Earlier, the 1999 Chamoli (M_w = 6.6) and 2005 Kashmir (M_w = 7.6) earthquakes in the NW Himalayan region were studied using space geodetic techniques to
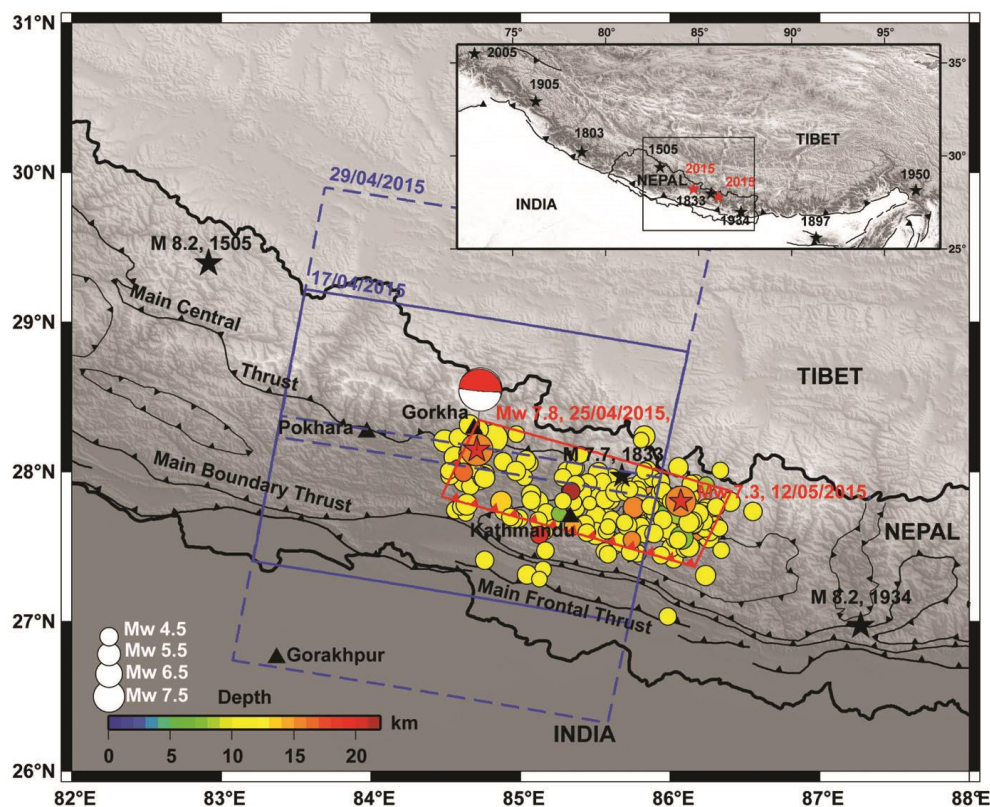
Figure 1. Topographical map showing the location of epicentres of M_w 7.8 and 7.3, Nepal earthquakes of 12 May 2015 (red stars) along with aftershocks in circles and historic/past and great/large earthquakes as black stars. The colours of the circles represent the hypocentral depths and different sizes indicate magnitudes. The focal mechanism solution (GCMT) of the 25 April 2015 event is shown as a beach ball. Footprints of Sentinel-1 data acquired on 17 April 2015 (blue line) and 29 April 2015 (blue dashed line) are superimposed. The thick blue-coloured rectangle represents a map view of the model fault plane (Figure 4). Major thrust faults, viz. Main Frontal Thrust (MFT), Main Boundary Thrust (MBT) and Main Central Thrust (MCT) in the study area are shown as black lines. (Inset) Map representing the present study area in a rectangle with great and large earthquakes since 1505 as stars and Indian plate boundary in black line.

determine their respective co-seismic displacements[8–10]. In this study we use synthetic aperture radar interferometry (InSAR) to map the co-seismic surface deformation caused by the $M_w = 7.8$, Gorkha earthquake and thereby to infer source parameters of the earthquake using elastic half-space modelling.

The ~2500 km long Himalayan arc evolved as a result of the collision between Indian and Eurasian plates since 60–50 Ma, and is one of the most seismically active continental collision zones in the world. The continental collision followed by under-thrusting of a part of the Indian continental crust, overriding of a part of the Eurasian plate, folding and faulting were responsible for the growth and emergence of the mountain topography and several earthquakes along the entire Himalayan arc. The long-term crustal shortening in the Himalaya is accommodated in a southward-propagating thrust fault consisting of three main thrust fault systems, namely Main Central Thrust (MCT), Main Boundary Thrust (MBT) and Main Frontal Thrust (MFT), which progressively emerged at different stages[11,12]. The southernmost thrust,

MFT, is now considered to be the most active of the three and delineates the northern limit of the exposed Indian plate (Figure 1). According to a conceptual tectonic model based on various geophysical data, it is suggested that MCT, MBT and MFT are connected to a detachment boundary known as the Main Himalayan Thrust (MHT) at a depth of 17–22 km (refs 6, 13). MHT flattens beneath the Lesser Himalaya and forms a mid-crustal ramp at the front of the Higher Himalaya[14]. During the active thrusting of India under the Tibetan Plateau, MHT is known to absorb about 20 mm/yr convergence in Nepal, which is nearly half the present convergence rate between India and Eurasia[15–18]. The elastic strain energy thus stored during the interseismic period is released periodically due to earthquakes causing rupture along the interseismically locked, brittle upper part of the MHT system beneath the outer and lesser Himalaya, which is characterized by a southern frontal ramp (MFT)[6,7,19,20]. Whereas, aseismic slip induces stress accumulation at zones beneath the higher Himalaya, which triggers intense micro-seismic activity and elastic strain in the
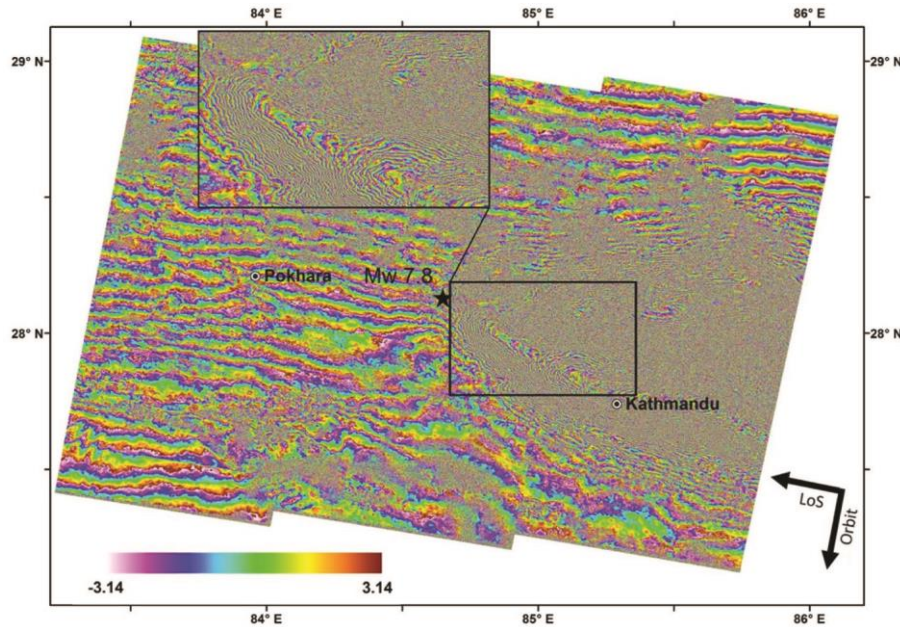
Figure 2. Co-seismic interferogram of the Gorkha earthquake. Each interferometric fringe ($-\pi$ to $+\pi$) corresponds to about 2.8 cm movement along the line-of-sight (LOS) of the satellite. Subset of the interferogram east of the epicentre (black star) is shown as inset map.

upper crust[13]. Hence, large-magnitude earthquakes are mostly confined to the basal thrust of MHT, which is close to the locked zone[21].

Co-seismic interferogram was generated using Sentinel-1 SAR data acquired during the descending passes on 17 and 29 April 2015. The interferogram was unwrapped and the topographic phases were removed using Shuttle Radar Topographic Mission (SRTM) data. The residual phases were converted to line-of-sight (LOS) displacement and geocoded to produce the co-seismic deformation map. The interferogram was detrended to reduce effects of orbital and ionospheric perturbations. The co-seismic interferogram has high coherence (mean ~ 0.3) owing to its short temporal separation (12 days) and low baseline (37 m). This indicates that the effect of topography and surface changes between the data acquisitions are minimum, and the deformation map generated could be confidently attributed to the co-seismic deformation. Further, the post-earthquake data were acquired three days after the main shock, and hence the effect of postseismic deformation on the interferogram is expected to be minimum.

Figure 2 presents the co-seismic interferogram of the 2015 Gorhka earthquake. The interferometric fringe pattern and fringe rate variation along the satellite direction clearly indicate surface deformation associated with the earthquake. The variation of fringes across the epicentral region is fairly smooth with reasonably good coherence (~0.3), which indicates that the rupture of the earthquake has not reached (broken) the surface. The deformation map generated from the interferogram (Figure 3) suggests an upliftment of about 1 m near Kathmandu and a subsi-

dence of about 0.8 m towards north along the LOS of the satellite. The broad wavelength of the deformation signals (~100 km) suggests co-seismic slip in the deeper parts of the causative fault plane. It is interesting to note that maximum amount of deformation occurred east–southeast of the epicentre. This is consistent with the distribution of aftershocks and clearly indicates east–southeastward propagation of the subsurface rupture, as suggested by the inversion of teleseismic data[2,22–24]. Further, an attempt has been made to map the deformation caused by the $M_w = 7.3$ aftershock which occurred on 12 May 2015, using ascending track Sentinel-1 data acquired on 5 and 15 May 2015. The $M_w = 7.3$ event caused displacement of about -0.4–0.6 m in the LOS direction (Figure S1, see Supplementary Material online). However, partial coverage of InSAR data limits detailed analysis and further modelling of the aftershock data.

We model the earthquake as a planar dislocation buried in elastic half-space[25,26]. The input parameters to the model are orientation (strike, dip and rake) and size (length, width and slip) of the rectangular fault. The model computes deformation at the surface with respect to the location and depth of the fault centriod. Fault parameters obtained from the waveform inversion model were used as initial constraints for modelling the surface deformation[1]. The geometry of the fault plane is optimized assuming uniform slip and looking for a minimum misfit with the InSAR data. The modelled deformation has been projected to the LOS of the satellite to compare with the observed deformation. We changed depth, dip and slip of the fault and generated a series of models to select the best-fit model which can reasonably explain the
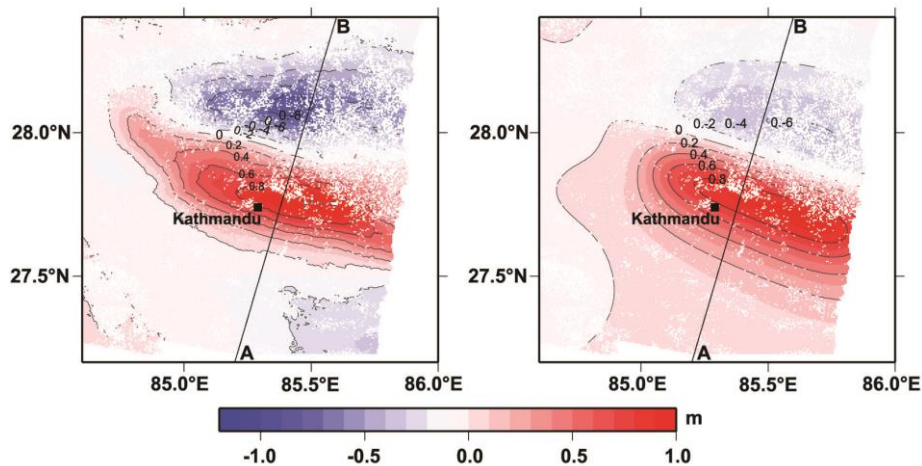
Figure 3. InSAR-derived (left) and model predicted (right) LOS deformation maps of the M_w 2015 Gorkha earthquake. Black lines show location of the profile drawn in Figure 4.
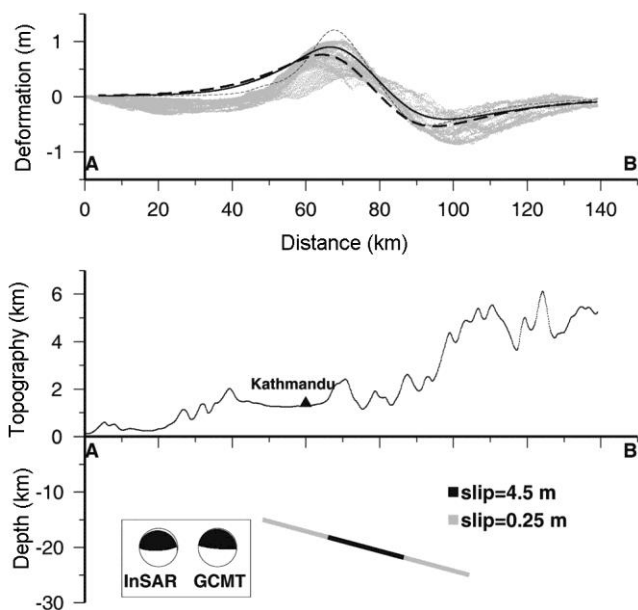

Figure 4. (Top) LOS deformation along profile AB (±50 km either side) shown as grey dots. Black line indicates the best fit modelled deformation along the profile AB (dip = 15° and depth 20 km). Deformation models along the profile AB for dip = 7° depth 20 km (dashed line), as well as dip 15° and depth = 12 km (dotted line) are shown for comparison. The topography along the profile (middle) and trace of model fault (bottom) are shown. Fault plane solutions obtained from InSAR and those of GCMT are also shown in the bottom panel.

amplitude and shape of the observed InSAR deformation pattern. We find that the length ($L = 170$ km), width ($W = 60$ km) and strike (286°) of the fault plane are well constrained by the orientation and shape of the observed deformation pattern. ALOS-2 interferogram[27] has also been considered to determine L and W, as the Sentinel-1 interferogram did not cover the easternmost extent of the deformation pattern (Figures 1 and 3).

Our initial models with parameters of uniform slip 2–4 m along a fault plane area of 170×60 sq. km, dip 7–

20°, and depth 5–30 km could not completely explain the observed deformation pattern, particularly the subsided area towards north. The wavelength of the model deformation pattern appears to be broader than that observed for greater depths, whereas amplitude of the deformation signal overestimates for shallower depths. This clearly indicates that the slip along the 170×60 sq. km fault plane is not uniform. An attempt has been made to model the deformation with a non-uniform slip, with a large amount of slip confined to a smaller fault patch within the major fault plane. We varied the width (10–40 km) and length (50–100 km) of the fault patch and searched for the best-fit model over a range of slip values. Our best-fit model consists of 4.5 m slip confined to the centre fault patch of size 95×22 sq. km and 0.25 m for the rest of the fault plane (Figure 4). The best-fit fault plane has a dip = 15° and rake = 98° with fault centroid at 85.45°E and 27.85°N located at a depth of 20 km. We notice that models with shallow depth (<20 km) clearly underestimate the wavelength of the deformation signal (Figure 4). From the best-fit fault plane we estimated the earthquake moment released during the 25 April 2015 Gorkha, Nepal event as 5.2×10^{20} Nm. This corresponds to a magnitude of $M_w = 7.75$, which closely matches with the estimation obtained from seismic waveform inversion magnitude ($M_w = 7.8$).

The InSAR data and model do not suggest surface rupture due to this earthquake despite having large magnitude and shallow hypocentre. However, recent palaeo-seismological data showed that the 1934 Nepal–Bihar and the AD 1255 earthquakes did rupture the surface, leaving the fault trace on the surface south of Kathmandu[3,28]. The 2005 Kashmir earthquake was also associated with a prominent surface rupture[8]. This clearly indicates the diversity in tectonics associated with great and large Himalayan earthquakes, as pointed out by Kayal[20,29].

Elastic dislocation model suggests that most of the slip (4.5 m) occurred on a fault patch of size 95×22 sq. km at

a depth ranging from 17 to 22 km (Figure 4), with less slip (0.25 m) on the surrounding part of the fault plane. The projected slip on the surface correlates with the coseismic deformation and surface topography. The moment magnitude estimated from our model closely matches with that estimated from teleseismic data. The modelled slip value on the fault is comparable with the average of the distributed slip values (0–6 m) derived using inversion of InSAR and GPS data by Lindsey *et al.*[27], and Wang and Fialko[30], though their model has shallower dip (7–10°). However, we notice that the steeper dip angle ~15° obtained in the present study is analogous to that of Sreejith *et al.*[31]. A more detailed discussion on the implications of steeper dip angle on earthquake nucleation in frontal Himalaya is provided later in the text. The hypocentral depth obtained using teleseismic data is 8–15 km (refs 1, 2). The mismatch in depth estimation between InSAR and teleseismic data is expected considering the varied assumptions involved in InSAR and seismic modelling approaches, particularly the earth model adopted and the use of a point or planar source[32]. Further, uncertainties involved in depth estimation using teleseismic data may be high in the Himalayan region due to local variations in seismic velocity leading to discrepancy in depth estimation between InSAR and seismic data[33], and structural heterogeneities existing in the underthrusting Indian plate[34].

The well-accepted hypothesis for large and great earthquakes in central Himalaya includes release of interseismic strain energy along the interseismically locked portion of the MHT[18,19,35]. Recent geodetic data suggest that during the interseismic period, aseismic thrust displacement occurs in the deeper and ductile northern part of the MHT alone, while no slow earthquakes have been detected in the brittle, external locked part of the MHT[15,17,18,36,37]. It is thus interesting to note that the area, depth and dip of our modelled fault plane are fairly consistent and overlap with the location of mid-crustal ramp in MHT with a dip angle ~16° at a depth of 10–25 km imaged from the seismic reflection and receiver function stacking[38,39]. Godard and Burbank[40] suggested that one of the most important parameters that controls strain partitioning in central Himalaya is the dip angle of the thrust faults in the MHT system. The 1999 Chamoli earthquake exemplifies such an out-of-sequence event along a fault that dips ~15° northwards[10]. Experimental studies also suggest that in the case of dip-slip earthquakes, the rupture propagation is primarily controlled by the dip angle and density of the overburden rocks[41].

The comparatively steeper dip angle, depth and location of the fault centroid fairly coincide with the mid-crustal ramp in central Nepal (Figures 1 and 4)[35]. This mid-crustal ramp, which connects the shallow section of the seismically active detachment in the south to the aseismically slipping deeper section in the north, is hence pivotal in earthquake generation with a potential to initi-

ate multistage rupture processes[23]. Therefore, portion of the MHT where the mid-crustal ramp interacts with the shallow locked fault segment seems to spawn earthquakes. As a consequence, the locked portion of the MHT along the mid-crustal ramp could have yielded the Gorkha earthquake that propagated east–southeast of the hypocentre[22]. The high conductivity zone characterized by intense micro-seismicity deduced from magnetotelluric and seismological data also supports the role of mid-crustal ramp, which must have acted as a barrier for stress build-up in central Nepal Himalaya[13,42]. Nevertheless, we suggest that the combination of unreleased background store of energy and the strain energy accumulated since the release of high tectonic stresses associated with the 1934 Nepal–Bihar earthquake would have triggered the 25 April 2015 Gorkha, Nepal earthquake. This also testifies possible presence of seismic gaps in the region as enunciated earlier by several researchers[7,19,43]. A realistic nonlinear slip distribution model and variable dip angles along the fault plane may be required to further fortify these observations and models.

Major conclusions of the present study are as follows.

(1) The 25 April 2015, M_w = 7.8 Gorkha, Nepal earthquake is associated with about 100 × 100 sq. km surface deformation and ~1 m upliftment near Kathmandu, and ~0.8 m subsidence towards north along LOS of the satellite. The maximum deformation caused by the earthquake is about 40 km east of the epicentre, suggesting an east–southeastward propagation of the rupture.

(2) Elastic dislocation modelling revealed that the rupture occurred on a north-dipping fault (dip = 15°) with length 170 km and width 60 km along the strike (286°). The model suggests large amount of slip (4.5 m) confined to the centre (95 × 22 sq. km) and less slip (0.25 m) on the surrounding parts of the fault plane.

(3) The moment release and magnitude estimated from the model are 5.2×10^{20} Nm and M_w 7.75 respectively, and closely match with the magnitude of seismic waveform observations.

(4) The area, depth and dip of the modelled fault plane are fairly consistent and overlap with the location of mid-crustal ramp in the MHT, which is pivotal in earthquake generation.

(5) The present study suggests that the 25 April 2015 Gorkha, Nepal earthquake would have been triggered due to the combined release of stored background energy and inter-seismic strain energy accumulated in the comparatively steeply dipping mid-crustal ramp along the MHT caused by the high plate boundary stresses since the 1934 Nepal–Bihar earthquake.

1. US Geological Survey National Earthquake Information Center Catalogue (USGS-NEIC). 2015; http://earthquake.usgs.gov/earthquakes/eventpage/us20002926.
2. Global Centroid Moment Tensor Catalogue (GCMT). 2015; http://www.globalcmt.org/CMTsearch.html.

3. Sapkota, S. N., Bollinger, L., Klinger, Y., Tapponnier, P., Gaudemer, Y. and Tiwari, D., Primary surface ruptures of the great Himalayan earthquakes in 1934 and 1255. *Nature Geosci.*, 2012, **6**, 71–76.

4. Paramesswaran, R. M., Natarajan, T., Rajendran, K., Rajendran, C. P., Mallick, R., Wood, M. and Lekhak, H. C., Seismotectonics of the April–May 2015 Nepal earthquakes: an assessment based on the aftershock patterns, surface effects and deformational characteristics. *J. Asian Earth Sci.*, 2015, **111**, 161–174; doi: 10.1016/j.jseaes.2015.07.030.

5. Adhikari, L. P. *et al.*, The aftershock sequence of the 2015 April 25 Gorkha–Nepal earthquake. *Geophys. J. Int.*, 2015, **203**, 2119–2124; doi: 10.1093/gji/ggv412.

6. Seeber, L., Armbruster, J. G. and Quittmeyer, R., Seismicity and continental subduction in the Himalayan Arc. In *Zagros, Hindu Kush, Himalaya, Geodynamic Evolution. Geodynamics Series* (eds Gupta, H. K. and Delany, F. M.), American Geophysical Union, Washington DC, 1981, vol. 3, pp. 215–242.

7. Bilham, R., Gaur, V. K. and Molnar, P., Himalayan seismic hazard. *Science*, 2001, **293**, 1442–1444.

8. Avouac, J.-P., Ayoub, F., Leprince, S., Konca, O. and Helmberger, D. V., The 2005, M_w 7.6 Kashmir earthquake: sub-pixel correlation of ASTER images and seismic waveforms analysis. *Earth Planet. Sci. Lett.*, 2006, **249**(3–4), 514–528; doi: 10.1016/j.epsl.2006.06.025.

9. Pathier, E., Fielding, E. J., Wright, T. J., Walker, R., Parsons, B. E. and Hensley, S., Displacement field and slip distribution of the 2005 Kashmir earthquake from SAR imagery. *Geophys. Res. Lett.*, 2006, **33**, L20310; doi: 10.1029/2006GL027193.

10. Satyabala, S. P. and Bilham, R., Surface deformation and subsurface slip of the 28 March 1999 M_w = 6.4 west Himalayan Chamoli earthquake from InSAR analysis. *Geophys. Res. Lett.*, 2006, **33**, L23305; doi: 10.1029/2006GL027422.

11. Hodges, K. V., Tectonics of the Himalayan and southern Tibet from two perspectives. *Geology*, 2000, **1123**, 324–350.

12. Rajendran, C. P., John, B. and Rajendran, K., Medieval pulse of great earthquakes in the central Himalaya; viewing past activities on the frontal thrust. *J. Geophys. Res.*, 2015, **120**, 1623–1641; doi: 10.1002/2014JB011015.

13. Pandey, M., Tankudar, R., Avouac, J.-P., Lavé, J. and Massot, J.-P., Interseismic strain accumulation on the Himalayan crustal ramp, Nepal. *Geophys. Res. Lett.*, 1995, **22**, 751–754.

14. Cattin, R. and Avouac, J.-P, Modeling mountain building and the seismic cycle in the Himalaya of Nepal. *J. Geophys. Res.*, 2000, **105**, 13389–13407.

15. Larson, K. M., Bürgmann, R., Bilham, R. and Freymueller, J. T., Kinematics of the India–Eurasia collision zone from GPS measurements. *J. Geophys. Res.*, 1999, **104**, 1077–1093.

16. Lavé, J. and Avouac, J.-P., Active folding of fluvial terraces across the Siwaliks Hills, Himalayas of central Nepal. *J. Geophys. Res.*, 2000, **105**, 5735–5770.

17. Bettinelli, P., Avouac, J.-P., Flouzat, M., Jouanne, F., Bollinger, L., Wills, P. and Chitrakar, G. R., Plate motion of India and interseismic strain in the Nepal Himalaya from GPS and DORIS measurements. *J. Geodesy.*, 2006, **80**, 567–589; doi: 10.1007/s00190-006-0030-3.

18. Ader, T. *et al.*, Convergence rate across the Nepal Himalaya and interseismic coupling on the Main Himalayan Thrust: implications for seismic hazard. *J. Geophys. Res.*, 2012, **117**, B04403; doi: 10.1029/2011JB009071.

19. Mugnier, J.-L., Gajurel, A., Huyghe, P., Jayagondaperumal, R., Jouanne, F. and Upreti, B., Structural interpretation of the great earthquakes of the millennium in the central Himalaya. *Earth-Sci. Rev.*, 2013, **127**, 30–47.

20. Kayal, J. R., Seismotectonics of the great and large earthquakes in Himalaya. *Curr. Sci.*, 2014, **106**, 188–197.

21. Avouac, J.-P., Bollinger, L., Lavé, J., Cattin, R. and Flouzat, M., Le cycle sismique en Himalaya, *C. R. Acad. Sci.*, 2001, **333**, 513–529.

22. Avouac, J.-P., Meng, L., Wei, S., Wang, T. and Ampuero, J.-P., Unzipping lower edge of locked Main Himalayan Thrust during the 2015, M_w 7.8 Gorkha earthquake, Nepal. *Nature Geosci.*, 2015, **8**, 708–711.

23. Fan, W. and Shearer, P. M., Detailed rupture imaging of the 25 April 2015 Nepal earthquake using teleseismic P waves. *Geophys. Res. Lett.*, 2015, **42**, doi: 10.1002/2015GL064587.

24. Grandin, R., Vallée, M., Satriano, C., Lacassin, R., Klinger, Y., Simoes, M. and Bollinger, L., Rupture process of the M_w = 7.9 2015 Gorkha earthquake (Nepal): insights into Himalayan megathrust segmentation. *Geophys. Res. Lett.*, 2015, **42**, 8373–8382; doi: 10.1002/2015GL066044.

25. Okada, Y., Surface deformation due to shear and tensile faults in a half-space. *Bull. Seismol. Soc. Am.*, 1985, **754**, 1135–1154.

26. Feigl, K. L. and Dupré, E., RNGCHN: a program to calculate displacement components from dislocations in an elastic half-space with applications for modeling geodetic measurements of crustal deformation. *Comput. Geosci.*, 1999, **25**, 695–704.

27. Lindsey, E., Natsuaki, R., Xu, X., Shimada, M., Hashimoto, H., Melgar, D. and Sandwell, D., Line of sight deformation from ALOS-2 interferometry: M_w 7.8 Gorkha earthquake and M_w 7.3 aftershock. *Geophys. Res. Lett.*, 2015, **42**, doi: 10.1002/2015 GL065385.

28. Bollinger, L. *et al.*, Estimating the return times of great Himalayan earthquakes in eastern Nepal: evidence from Patu and Bardibas strands of the Main Frontal Thrust. *J. Geophys. Res.*, 2014, **119**, doi: 10.1002/2014JB010970.

29. Kayal, J. R., Himalayan tectonic model and the great earthquakes. *Geomat. Nat. Hazard Risk*, 2010, **1**, 51–67; doi: 10.1080/19475701003625752.

30. Wang, K. and Fialko, Y., Slip model of the 2015 M_w 7.8 Gorkha (Nepal) earthquake from inversions of ALOS-2 and GPS data. *Geophys. Res. Lett.*, 2015, **42**, 7452–7458; doi: 10.1002/2015-GL065201.

31. Sreejith, K. M., Sunil, P. S., Agrawal, R., Saji, A. P., Ramesh, D. S. and Rajawat, A. S., Coseismic and early postseismic deformation due to the 25 April 2015, Mw 7.8 Gorkha, Nepal earthquake from InSAR and GPS measurements. *Geophys. Res. Lett.*, 2016, **43**, 1–9; doi: 10.1002/2016GL067907.

32. Weston, J., Ferreira, A. and Funning, G. J., Systematic comparisons of earthquake source models determined using InSAR and seismic data. *Tectonophysics*, 2012, **532–535**, 61–81.

33. Satyabala, S. P., Yang, Z. and Bilham, R., Stick–slip advance of the Kohat Plateau in Pakistan. *Nature Geosci.*, 2012, **5**, 147–150.

34. Gahalaut, V. K. and Arora, B. R., Segmentation of seismicity along the Himalayan arc due to structural heterogeneities in the under-thrusting Indian plate and overriding Himalayan wedge. *Episodes*, 2012, **354**, 493–500.

35. Grandin, R., Doin, M.-P., Bollinger, L., Pinel-Puyssegur, B., Ducret, G., Jolivet, R. and Sapkota, N., Long-term growth of the Himalaya inferred from interseismic InSAR measurements. *Geology*, 2012, **4012**, doi: 1059–1062; doi: 10.1130/G33154.1.

36. Bilham, R., Larson, K., Freymueller, J. and Project Idylhim members, GPS measurements of present day convergence across the Nepal Himalaya. *Nature*, 1997, **386**, 61–64.

37. Jouanne, F. *et al.*, Current shortening across the Himalayas of Nepal. *Geophys. J. Int.*, 2004, **157**, 1–14; doi: 10.1002/2014-JB010970.

38. Nabelek, J. *et al.*, The Hi-CLIMB Team, 2009. Underplating in the Himalaya–Tibet collision zone revealed by the Hi-CLIMB experiment. *Science*, 2009, **325**, 1371–1374.

39. Caldwell, W. B., Klemperer, S. L., Lawrence, J. F., Rai, S. S. and Ashish, Characterizing the Main Himalayan Thrust in the Garhwal

Himalaya, India, with receiver function CCP stacking. *Earth Planet. Sci. Lett.*, 2013, **367**, 15–17.

40. Godard, V. and Burbank, D. W., Mechanical analysis of controls on strain portioning in the Himalayas of the central Nepal. *J. Geophys. Res.*, 2011, **116**, B10402, doi: 10.1029/2011JB008272.

41. Lee, J. W., Hamada, M., Tabuchi, G. and Suzuki, K., Prediction of fault rupture propagation based on physical model tests in sandy soil deposit. In 13th World Conference on Earthquake Engineering Vancouver, Canada, 1–6 August 2004, paper no. 119.

42. Lemonnier, C. *et al.*, Electrical structure of the Himalaya of Central Nepal: high conductivity around the mid-crustal ramp along the MHT. *Geophys. Res. Lett.*, 1999, **26**, 3261–3264.

43. Singh, D. D. and Gupta, H. K., Source dynamics of two great earthquakes of the Indian subcontinent: the Bihar–Nepal earthquake of 15 January 1934 and the Quetta earthquake of 30 May 1935. *Bull. Seismol. Soc. Am.*, 1980, **703**, 757–773.

44. Wessel, P. and Smith, W. H. F., New improved version of generic mapping tools released. *Eos Trans.*, 1998, **79**(47), 579; doi: 10.1029/98EO00426.

Rumen virome: an assessment of viral communities and their functions in the rumen of an Indian buffalo

Nidhi R. Parmar, Subhash J. Jakhesara, Amitbikram Mohapatra and Chaitanya G. Joshi*

Department of Animal Biotechnology,
College of Veterinary Science and Animal Husbandry,
Anand Agricultural University, Anand 380 001, India

Viruses play a key role in compensating bacterial population in any ecosystem of the planet. Rumen, a highly diverse ecosystem, is still under-explored for viral communities and their metabolic capabilities. We carried out shotgun sequencing of enriched viral particles from rumen fluid collected from an Indian buffalo. The study revealed that well-assembled contigs of Newbler and Velvet got majority of assignments to virus domain that further revealed *Caudovirales* as a major order. A majority of the Firmicutes bacteriophages were found in the study, which also confirm the presence of conserved domains such as peptidases against Firmicutes phages.

*For correspondence. (e-mail: cgjoshi@rediffmail.com)

Keywords: Bacteriophage, contigs, gene prediction, peptidase, virome.

THE rumen is a highly diverse environment encompassing bacteria, archaea, eukaryota and viruses. Several studies have examined the structure of rumen bacterial communities with insight into their efficiency of carbohydrate utilization[1,2]. Additionally, numerous new fungal communities have been reported using 18S r-RNA gene[3]. Despite their global abundance[4], the viral communities are still underexplored from any particular niche. Various microbial ecosystems such as soil associated ecosystem[5], aquatic microbial ecosystem[6] and gut microbial community[7] have been studied for viruses using conventional methods.

With the advent of next generation sequencing (NGS) technology, it has now become easier to efficiently study the viral community from any niche at greater depth even if their host bacterium is uncultivable. Although there are many reports that have deciphered the viral community in bovine rumen including phage–bacteria relationship[8,9], so far no study involving exploration of the viral community from Indian ruminants has been reported. The present study attempts to enrich bacteriophages from the rumen of an Indian buffalo, with further exploration of taxonomy of rumen virome, the probable hosts and the rumen virome metabolic profile.

The present study included a Surti breed of buffalo reared at Animal Nutrition and Research Station (ANRS), Anand Agricultural University (AAU), Anand, the diet of which mainly included forage-based diet before sample collection. All experimental procedures involving animals were conducted with prior approval by the University Animal Ethics Committee (permit number: AAU/GVC/CPCSEA-IAEC/108/2013), Anand Agricultural University (AAU), Anand, Gujarat, India.

Rumen fluid (~500 ml) was collected using flexible stomach tube after 2 h of feeding[10]. The rumen fluid was brought to laboratory under refrigerated condition after fractionation using two-layered muslin cloth to remove larger solid particles of feed. First, 100 ml of rumen fluid was centrifuged at 5000 g for 10 min, to remove larger particles. The supernatant was collected and filtered with 3 μm filter followed by centrifugation at 5000 g for 10 min. Again, the supernatant was filtered through 0.22 μm filter and transferred into two Vivaspin 20, 30 kDa molecular weight cutoff columns (~15 ml each) for centrifugation at 8000 g for 15 min and the particles above 30 kDa were enriched by retaining 1 ml of the concentrate from top of the column[11]. The concentrate was then given DNase I (at final concentration of 10 μg/ml) and RNase A (at final concentration of 10 μg/ml) treatment for 1 h at 37°C followed by enzyme inactivation at 65°C for 10 min.

Total DNA from the nuclease-treated rumen virome concentrate was isolated using High Pure Viral Nucleic